The simultaneous synthesis of carbon dots and carbon spheres with tunable sizes using a vertical chemical vapour deposition method

Lerato L Mokoloko[a], Roy P Forbes[a] and Neil J Coville[a*]

[a]*DSI-NRF Centre of Excellence in Catalysis and the Molecular Sciences Institute, School of Chemistry. University of the Witwatersrand, Johannesburg, South Africa.*

Received 05 April 2021, revised 29 September 2021, accepted 09 November 2021

ABSTRACT

Herein we report on the direct synthesis of solid hydrophobic carbon dots (CDs) and simultaneously carbon spheres (CSs), using a vertical chemical vapour deposition (CVD) reactor. The HRTEM data indicated that the CDs and CSs originated from different carbon building blocks indicated that the CDs and CSs originated from different carbon building blocks. The CDs were obtained by reacting acetylene (C_2H_2) and Ar mixtures at high flow rates (≥500 sccm) and high temperatures (800–1000 °C). TEM studies indicated that the CDs produced were graphene-like quantum dots that increased in size from *c.* 3 nm to 8 nm as the Ar flow rate (constant C_2H_2 flow rate) was decreased, while small solid CSs (*c.* 100 nm) were also synthesised in the process. The CSs had a typical spherical layered structure with no graphitic core. A mechanism to rationalise the observation that the CDs and CSs grew simultaneously by different pathways with no formation of intermediate-sized particles is given.

KEYWORDS

carbon dots, chemical vapour deposition, nanostructure, spectroscopy

INTRODUCTION

Carbon dots (CDs) are described as carbonaceous nanoparticles composed of discrete, quasi-spherical structures with particle sizes below 10 nm. They have been a subject of interest, particularly due to their extraordinary fluorescence properties - a characteristic that is not very common for carbon-based nanomaterials[1–3]. In addition, their size- and luminescence-dependent behaviour is similar to the properties known for conventional metal-based quantum dots. However, unlike the metal-based quantum dots, CDs have high stability, low production cost, low toxicity, good biocompatibility and can also be produced in high abundance.[3] It is because of these properties that CDs have been used for application in bioimaging, [4,5] biosensing,[5,6] water purification,[7] photocatalysis,[8,9] solar cells,[10] and various other systems.

Many synthesis methods have been developed and optimised to produce CDs with *hydrophilic* surface functionalities,[11] but only a few methods have been developed for the synthesis of *hydrophobic* CDs. The two most commonly used routes to synthesise CDs that contain *hydrophobic* groups usually involve reacting a carbon source with a hydrophobic capping agent[12–15] or post modification of functionalised CDs with an amino dopant.[16] Another method to produce *hydrophobic* CDs is by carbonising a non-functionalised carbon source that contains only C and H atoms such as C_2H_2,[17,18] toluene,[19,20] or natural gas.[21] The *hydrophobic* properties can also be conferred by the post-reaction removal of all functional groups from the CD surface.

The carbonisation of C_2H_2 in a CVD reactor has been extensively studied for the synthesis of carbon nanomaterials such as graphite, graphene, fullerene, carbon nanotubes (CNTs) and carbon spheres (CSs).[22–26] These carbon materials show interesting surface chemistry, electronic properties, degree of graphitisation and thermal stabilities that can be varied and made suitable for tailored applications.[22–26] Surprisingly, to date only a few reports have highlighted the synthesis of CDs using the CVD reaction. Yan et al.[17] reported the synthesis of CDs using a horizontal CVD method for the first time. CDs with an average particle size of *c* 3.5 nm were produced using C_2H_2 as a carbon source and argon (Ar) as a carrier gas.[17,18]

To expand on the CVD approach, we have investigated the use of a *vertical* CVD method, using C_2H_2 as the carbon source and different Ar flow rates, to synthesise CDs with controlled particle sizes. Reports have shown that carbon spheres (CSs) with tuneable sizes can be synthesised using this *vertical* CVD method.[24] This method limits the growth of the carbon and consequently should make it possible to obtain CDs with controlled sizes. To the best of our knowledge, the synthesis of CDs with particle size control using the vertical CVD method is a novel approach to making CDs. To gain more insight into the properties of these new CDs, they were characterised using electron microscopy, spectroscopy and thermal analysis was undertaken. The properties of these CDs were compared with those obtained using the horizontal CVD method. CSs with a narrow size was also produced and analysed using this methodology.

METHODS

Materials

Acetylene gas (C_2H_2, 99.99%) and argon gas (Ar, 99.9%) were supplied by Afrox, South Africa. Reagent grade toluene ($C_6H_5CH_3$, 99.5%) was purchased from Sigma-Aldrich, South Africa.

Synthesis procedure

The synthesis procedure followed here is a modification of a procedure reported by Mutuma et al.[24] for the synthesis of solid CSs using a vertical CVD reactor under atmospheric pressure. In a typical reaction set-up, a vertical CVD reactor fitted with a quartz tube (2.4 cm i.d. × 1.15 m length) and a 3-L round-bottom flask (RBF) was used as a sample collection chamber (SCC#1), as shown in Figure 1. For the collection of CDs, a bubbler containing toluene was used as a second sample collection chamber (SCC#2). Ar gas was passed through the quartz tube as the reactor was heated at 10 °C min^{-1}. When the desired temperature of the reaction was reached, C_2H_2 gas from a second delivery line (see Figure 1) was introduced to the reactor, and the reaction was allowed to proceed for 2 h. The C_2H_2 gas flow was kept constant at 25 sccm in all experiments. The temperature was held at 1000 °C in the initial experiments. After 2 h, SCC#2 contained a mixture of carbon products, including CDs, while SCC#1 contained

*To whom correspondence should be addressed
Email: neil.coville@wits.ac.za

ISSN 1996-840X Online / South African Chemical Institute / http://saci.co.za/journal

https://doi.org/10.17159/0379-4350/2022/v76a05

mostly CSs. The mixture from SCC#2 (see Figure S1 for the product before any purification) was sonicated for 1 h. After that, it was centrifuged at 15 000 rpm and subsequently syringe filtered through a 0.45 µm polytetrafluoroethylene (PTFE) filter to further remove larger agglomerates. A rotary evaporator was then used to remove the toluene at 80 °C. The product from SCC#1 was collected and then purified using Soxhlet extraction in 200 mL toluene at 120 °C for 24 h. The products were then dried in an oven at 80 °C. Other syntheses were also conducted at different temperatures and flow rates. Table 1 details the temperature, Ar flow rate used and synthesis percent yield obtained for each synthesis of the CDs and CSs. The samples obtained were denoted according to their type (CDs or CSs), and with subscripts that represent the Ar flow rate (in sccm), the temperature (×100, in °C) and the collector (SCC#), respectively. For example, the CDs were named $CDs_{520/10/2}$, when an Ar flow rate of 520 sccm, T = 1000 °C, and collector #2 were used.

Characterisation

The particle size distribution and morphology of the as-prepared CDs and CSs were determined by transmission electron microscopy (TEM) using an FEI G2 TECNAI Spirit T12 instrument operated at 120 kV. A JEOL JEM 2100 high-resolution transmission electron microscopy (HRTEM) fitted with a LaB6 gun was used for high-resolution imaging. Powder X-ray diffraction (PXRD) patterns were determined using a Bruker D2 phaser X-ray diffractometer equipped with a $Cu_{K\alpha 1/2}$ X-ray radiation source (λ = 1.54060 Å). Raman and photoluminescence (PL) spectroscopy measurements were conducted using a Horiba LabRAM HR micro-Raman spectrometer coupled with a PL excitation laser of 245 nm (Lexel Model 95 SHG argon ion laser). Ultraviolet-visible (UV-vis) spectroscopy analyses were carried out on an Agilent Technologies Cary (100) Series UV-vis spectrophotometer, using a tungsten halogen light source. The samples were excited at 365 nm. Infrared (IR) spectra were collected using a Brucker TENSOR 27 Fourier transform infrared (FTIR) spectrometer. The CDs' and CSs' thermal stability were determined using a Perkin Elmer Pyris STA6000 thermal gravimetric analyser (TGA). The samples were subjected to temperatures ranging from 35 to 900 °C, at a ramp rate of 10 °C min^{-1}. N_2 gas (20 sccm flow rate) was used as a purge gas, and air (10 sccm) as an analysis gas.

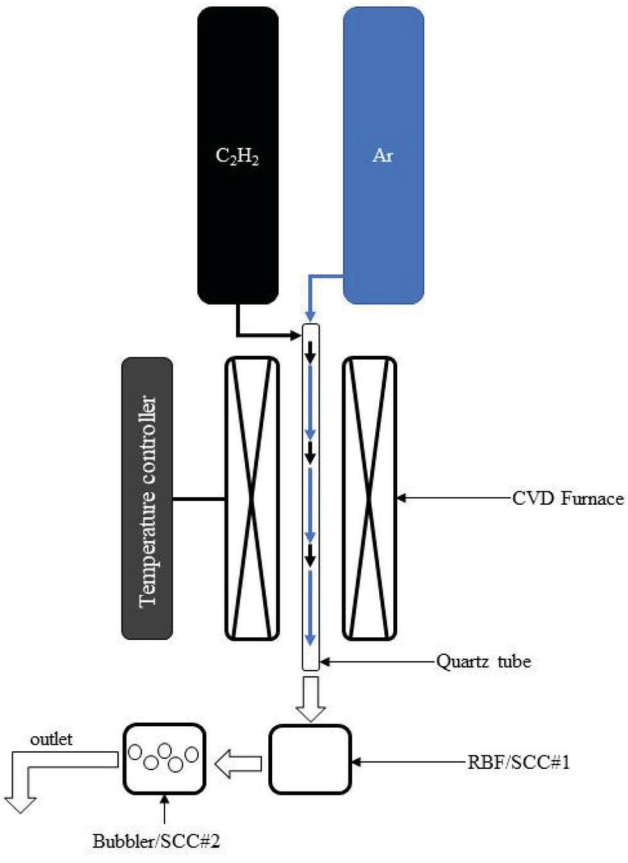

Figure 1: Illustration of the reactor used to make and collect the CDs (and CSs) from C_2H_2 using the vertical CVD method

RESULTS AND DISCUSSION

CDs with different particle sizes were synthesised using a simple "bottom-up" approach using a vertical CVD reactor under atmospheric pressure. The reaction involved the carbonisation of C_2H_2, a non-functionalised carbon precursor, at a high temperature that directly produced hydrophobic CDs. In preliminary studies, many experiments were performed to evaluate the collection of the CDs. Eventually, through trial and error, a high Ar flow rate (500–600 sccm), a low C_2H_2 flow rate (25 sccm) and high temperatures (≥800 °C) were chosen for the study. However, even using these conditions, CSs were still produced with the CDs. For the syntheses conducted >800 °C (>500 sccm Ar), the CSs products were mainly collected in the first collector (SCC#1) at the bottom of the CVD reactor. In contrast, the less dense (fluffy) and smaller products such as CDs and other carbon agglomerates were collected in SCC#2 in Figure 1. Other conditions produced only CSs in SCC#1 and SCC#2 and no CDs in SCC#2 (Table 1). Similar reactions performed at 700 °C yielded no CDs or CSs products.

Table 1: Parameters used for the syntheses of CDs and CSs and the resulting product yields and particle sizes

Sample notation[a]	Temperature (°C)	Ar flow rate (sccm)	Particle sizes (nm)	Yield (%)
$CSs_{600/10/1}$			105 ± 17	42.1
$CSs_{600/10/2}$	1000	600	110 ± 15	6.0
$CDs_{600/10/2}$			3 ± 1	2.4
$CSs_{550/10/1}$			105 ± 17	42.4
$CSs_{550/10/2}$	1000	550	109 ± 19	9.7
$CSs_{550/10/2}$			6 ± 2	4.3
$CSs_{520/10/1}$			107 ± 18	43.5
$CSs_{520/10/2}$	1000	520	109 ± 14	9.2
$CSs_{520/10/2}$			8 ± 2	5.1
$CSs_{400/10/1}$			108 ± 17	44.0
$CSs_{400/10/2}$	1000	400	95 ± 14	14.0
$CDs_{400/10/2}$			–	–
$CSs_{350/10/1}$			109 ± 16	44.7
$CSs_{350/10/2}$	1000	350	109 ± 17	17.7
$CDs_{350/10/2}$			–	–
$CSs_{600/9/1}$			110 ± 15	41.0
$CSs_{600/9/2}$	900	600	111 ± 27	8.0
$CDs_{600/9/2}$			3 ± 2	2.0
$CSs_{600/8/1}$			109 ± 18	34.5
$CSs_{600/8/2}$	800	600	110 ± 34	3.2
$CDs_{600/8/2}$			3 ± 2	0.9
$CSs_{400/8/1}$			322 ± 60	31.7
$CSs_{400/8/2}$	800	400	220 ± 23	15.2
$CDs_{400/8/2}$			–	–
No CSs	700	600	–	–
No CDs			–	–
No CSs	700	400	–	–
No CDs			–	–

[a] The notation used in the table describes the types of products obtained. The subscripts represent the Ar flow rate (in sccm), the temperature (×100, in °C) and the sample collection chamber (SCC# in Figure 1), respectively

The TEM images of the CDs products obtained in SCC#2 at different flow rates (together with their corresponding particle size distributions) are shown in Figure 2. The results show that the CDs are quasi-spherical in shape, well dispersed and have a narrow particle size distribution. The average particle sizes recorded for $CDs_{600/10/2}$, $CDs_{550/10/2}$ and $CDs_{520/10/2}$ were 3 ± 1 nm, 6 ± 2 nm and 8 ± 2 nm, respectively. This dispersion shows that as the flow rate of Ar gas was decreased, the resulting particle size increased. As more C_2H_2 is introduced into the reactor, the C species produced increased (as C_2H_2 decomposed) to form aggregates that grew, nucleated and crystallised into larger C nanoparticles.[17] Therefore, the increased carrier gas flow rate reduced the growth stage of the C aggregates and the formed particles were quickly transported into the collection chambers, resulting in the collection of smaller particles.

Only CSs were collected in SCC#1 at an Ar flow rate of 600, 550, 520, 400 and 350 sccm, and all the CSs were similar in particle size, as shown in Table 1. Thus, at 1000 °C (C_2H_2 = 25 sccm; Ar = 350–600 sccm), the CSs collected in SCC#1 show that the CS growth is little affected by the varying flow rates, and their average particle sizes are ~100–110 nm. At higher C_2H_2 flow rates, much larger CSs are formed.[24] The TEM image of the CSs product (named $CSs_{520/10/1}$, $CSs_{550/10/1}$ and $CSs_{600/10/1}$) obtained at Ar = 600 sccm are shown in Figure S2–4).

The HRTEM images of $CDs_{600/10/2}$ (Figure S5a)) show well-resolved lattice fringes with a lattice d-spacing of *c.* 0.21 nm, which is associated with the (100) facets of graphitic carbon[27]. The HRTEM images of the $CSs_{600/10/1}$ (Figure S5b) showed a highly amorphous material, with no lattice fringes observed. This observation indicates that these CSs are different from those found for the CDs. Particle growth of carbon black (CB) is similar to that for CSs growth and yields an amorphous core surrounded by concentric layers of short-length graphene-like sheets.

The effect of temperature on the particle sizes was also investigated. When the temperature was reduced from 1000 to 900 °C and 800 °C (C_2H_2 = 25 sccm; Ar = 600 sccm) the CDs formed had d = 3 ± 2 nm (Figure S6). The CSs size was also unaffected by the temperatures used. The effect of temperature was only detected at a low Ar flow rate (400 sccm) and a lower temperature (800 °C), where only CSs were collected with particle sizes of 322 ± 60 nm (SCC#1) and 220 ± 23 nm (SCC#2) (Figure S7 and S8). When the temperature was further decreased to ≤700 °C, no CDs or CSs were formed.

The percentage yields of the products are recorded in Table 1. The CDs were produced in low amounts (<5%) with the highest yields observed at 1000 °C. In contrast, good yields of CSs were formed (*ca.* 40%). The CDs formed are lightweight. To enhance the CD yield, a second bubbler was placed next to SCC #2 to collect any product that may have been lost by the rapid gas flow rates. However, for Ar flow rates between 520–600 sccm, the CDs yield only increased by ~0.5%.

The PXRD patterns of the CD and CS products (Figure 3a)) show broad peaks at *c.* 25° and *c.* 44° 2θ, which are attributed to the (002) and (101) planes of graphitic carbon, respectively[28]. The Raman spectra of the CDs (Figure S9a) show the Raman D-band (~1330 cm^{-1}) indicating the presence of sp^3 amorphous type carbon, and the G-band (~1595 cm^{-1}) arises due to the presence of sp^2 graphitic type carbon[29]. The resulting I_D/I_G ratios of the material were ~0.5, confirming the presence of substantial amounts of graphitic components[29]. The PL spectra (Figure 3b) showed that the CDs and not the CSs have optical properties. The $CDs_{600/10/2}$, $CDs_{550/10/2}$ and $CDs_{520/10/2}$ show a broad peak with blue to green emission in the visible light region,[30,31] with the peak maximum at *c.* 450 nm and a shoulder at *c.* 500 nm. Previous reports have indicated that the PL peak shifts to higher wavelengths when the particle sizes of functionalised CDs increase[32]. However, this was not the case with the CDs studied here. The TEM particle size distribution histograms of the CDs also showed that the nanoparticle ranges overlapped, suggesting an inhomogeneous composition of nanoparticles, leading to the broad peaks observed in the PL spectra. The CSs did not show any excitation activity at this excitation wavelength. The UV-vis spectra for $CDs_{600/10/2}$, $CDs_{550/10/2}$ and $CDs_{520/10/2}$ (Figure 3c) show strong absorptions in the UV region, similar to that observed for CDs synthesised using a horizontal CVD.[17] As with the PL spectroscopy analysis, the CSs did not show UV optical activity.

FTIR spectra (Figure S9b) of the $CDs_{600/10/2}$, $CDs_{550/10/2}$, $CDs_{520/10/2}$, $CSs_{400/10/2}$ and $CSs_{350/10/2}$ all had a similar pattern which showed the presence of weak C-H bonds (3000–2850 cm^{-1}, 1456–1377 cm^{-1}), C=C bonds (1668–1271 cm^{-1}), and C=O bonds (~1724 cm^{-1}). The C=O absorption peak indicates some functional groups present on

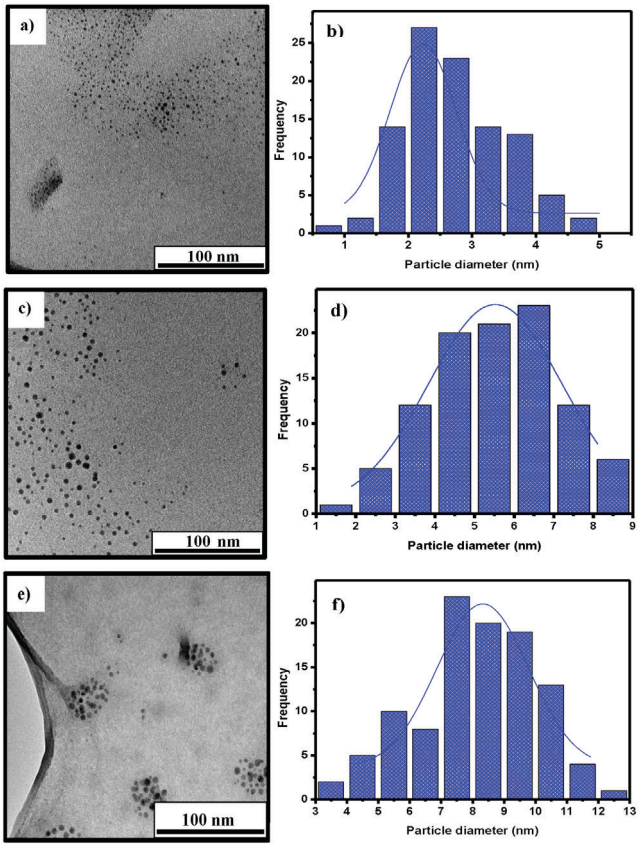

Figure 2: TEM images and particle size distribution histograms of CDs produced at 1000 °C and different argon flow rates **a-b)** $CDs_{600/10/2}$, **c-d)** $CDs_{550/10/2}$, **e-f)** $CDs_{520/10/2}$

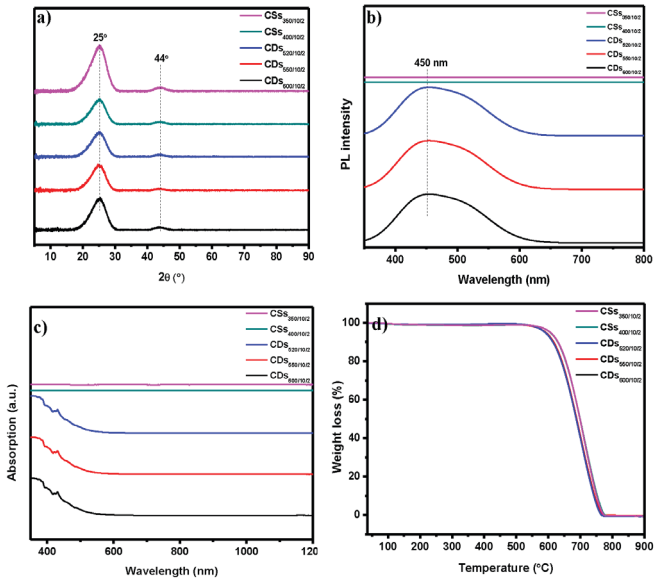

Figure 3: a) PXRD, **b)** PL, **c)** UV-Vis spectra, and **d)** TGA, data for $CDs_{600/10/2}$, $CDs_{550/10/2}$ and $CDs_{520/10/2}$, $CSs_{400/10/2}$ and $CSs_{350/10/2}$

the surface. When compared to the FTIR spectra of CDs produced by other routes,[33–35] it is clear that the CDs prepared here have fewer functional groups. To further confirm this, the dispersibility of $CDs_{600/10/2}$ in distilled water was investigated and compared with the CDs obtained from carbonising vitamin C in a microwave-assisted hydrothermal reaction following the reaction procedure reported by Mokoloko[36]. It was found that the $CDs_{600/10/2}$ were not dispersible in distilled water even after sonicating for 1 h, while the functionalised CDs (from vitamin C) dispersed readily in water even without sonication (Figure S10). The CDs are known to inherit some of the chemical makeup of their precursors. It is also the case with the CDs obtained from vitamin C. Vitamin C contains a significant number of O-functional groups, which makes it water dispersible. Likewise, the CDs were found to contain O-functional groups on their surface, and these were responsible for their water dispersibility.[36]

The thermograms in Figure 3d show that the materials decompose completely in air. The derivative weight loss of these thermographs is shown in Figure S11 and indicates the insignificant amount of surface functional groups on these CDs. CDs containing large amounts of functional groups show major thermal decomposition peaks between *c.* 200–500 °C.[33,34,37] The graphs show a small weight loss peak at *c.* 100 °C, which can be attributed to the loss of absorbed moisture. The decomposition of the CDs occurred between 701 °C and 711 °C. The decomposition temperatures of the CDs reported here are comparable to those reported for amorphous and graphitised carbon nanomaterials, such as CSs,[24] CNTs,[25] and CNOs.[38]

Although the synthesised CDs have different particle size distributions, there was no significant difference in their thermal, spectral and structural (PXRD) properties. Compared to CDs made by alternative procedures where large shifts in spectral properties were observed as a function of CD size and surface coverage.[39] It could be concluded that the key factor in the spectral variability of functionalised CDs must reside more with the surface functional groups rather than with their size.

The CDs produced in this study were compared to those produced utilising the horizontal CVD method.[17,18] It appears that the CDs all produce similar TEM, UV-vis and FT-IR data. The PXRD patterns, together with the HRTEM lattice fringes and the Raman spectra, suggested that our CVD method produced graphitic-like quantum dots, similar to those reported from the horizontal CVD method.[17] The advantage of using a vertical reactor relates to controlling the time that the CDs remain in the reactor. Thus, the method appears to be effective for the synthesis of (i) small and narrow sized CSs (≤100–320 nm), (ii) producing a good percentage yield of the CSs and (iii) providing a method to produce CDs with controlled size. This vertical reactor use makes it possible to produce CDs <5 nm using controlled temperature and flow rate conditions (from 70/700 sccm C_2H_2/Ar at 1000 °C[17,18] to 25/600 C_2H_2/Ar at 800–1000 °C).

CDs and CSs growth mechanism

One would expect that the CDs and CSs originate from common building blocks generated from the C_2H_2. Indeed, the Raman spectra, TGA data and PXRD patterns of both CDs and CSs appear to be identical. However, TEM data suggest otherwise.

1. The HRTEM images indicate graphite-like CDs,[40] while the CSs show no core made of graphene layers in a graphite arrangement (Figure S5).
2. The CDs made in a horizontal reactor also generate a graphene-like structure.[17,18] Thus, the important issue in making the CDs relates to the rapid removal of the CDs from the reactor. The use of a vertical CVD reactor allows this to be done in a controlled manner.
3. The general outline of the mechanism to grow CDs from fragments generated from C_2H_2 [17] would apply to the CDs made in the vertical reactor.
4. The sizes of the CDs and CSs as a function of Ar gas flow show no overlap (Figure 4). Indeed, the sizes show only a small change in size within each type, as the Ar flow rate varies. The observation of only two sizes of products implies two different growth mechanisms for the CDs and CSs from different building blocks.
5. At high temperatures, acetylene is well known to be transformed into polycyclic aromatic hydrocarbons (PAHs), consisting of fused hexagonal, pentagonal, and heptagonal carbon fragments.[41–43] In the case of CSs, pentagonal and hexagonal carbon fragments pair to form a spiral core and a spherical structure, which is terminated by graphitic flakes.[44,45] A cartoon showing the synthesis of the CSs (and CDs) from PAHs is given in Figure 5.
6. The CDs do not show this effect; they consist of stacked graphene layers, which implies that the ratio of C_6 planar rings to C_5/C_7 rings leads to the different structures seen. This stacking is associated with the different flow rates used, leading to different carbon growth patterns in the CVD reactor (Figure 5).
7. It is possible that a catalytic effect of the quartz tube could also play a role in generating the two different carbons formed.[41]

The unexpected finding suggests that it should be able to generate CDs in a much higher yield by controlling the CDs building blocks. This control could be done by adding benzene or related planar carbon sources to the C_2H_2.[43] Efforts in this direction are currently underway.

CONCLUSIONS

For the first time, this study reports the synthesis of CDs with different particle sizes (below 10 nm) made in a vertical CVD reactor. This method produced hydrophobic CDs in an *in-situ* method. The structural and electronic properties of the CDs were studied, and it was confirmed that the CDs are similar in their physical and optical properties to those produced by a horizontal CVD method. This similarity includes their quasi-spherical shape made of graphitic layers, UV-vis absorption properties resulting from π → π* transitions

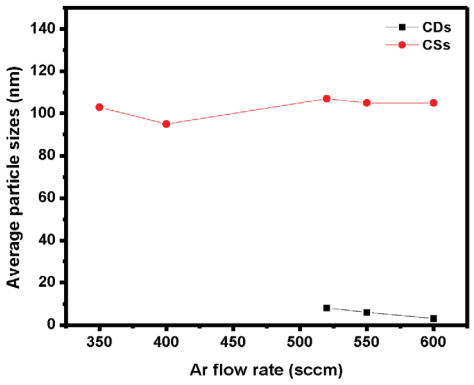

Figure 4: CDs and CSs particle sizes as a function of Ar flow rate at 1000 °C

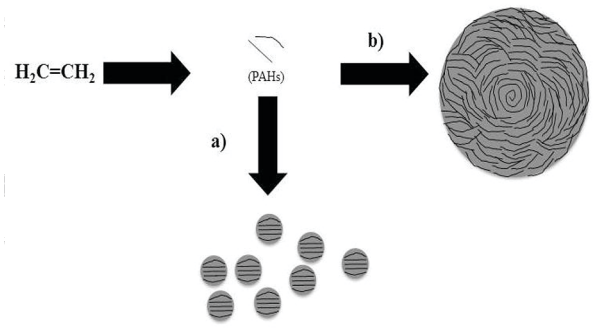

Figure 5: Possible mechanism to show growth of **a)** CDs and b) CSs from curved and planar PAHs.

and the presence of a limited number of functional groups as suggested by their FTIR spectra. The TGA results showed that these CDs have thermal stability similar to those reported for well-known carbon allotropes such as CSs, CNTs and CNOs. The data suggests that these CDs could be used in high-temperature applications. This method also produced small CSs (*ca.* 100 nm) with a narrow particle distribution and high thermal stability. Most importantly, it is clear that a different mechanism produces the CDs produced in this study than that used to make CSs.

ACKNOWLEDGEMENTS

We wish to thank the NRF, the University of the Witwatersrand and the DSI-NRF Centre of Excellence in Catalysis for financial support. We would also like to express our gratitude to Dr Rudolph Erasmus (School of Physics, University of the Witwatersrand, South Africa) for PL and Raman spectroscopy data and Rhandzu Rikhotso (Council for Scientific and Industrial Research, South Africa) for HRTEM data.

COMPETING INTERESTS

The authors have no competing interests

AUTHOR CONTRIBUTIONS

Conceptualisation (NJC, LM); Formal analysis (NJC, LM, RF) Funding acquisition (NJC, LM), Writing (NJC, LM, PF).

SUPPLEMENTARY MATERIAL

Supplementary information for this article is provided in the online supplement.

ORCID IDs

Lerato Mokoloko – https://orcid.org/0000-0003-4980-0319
Roy Forbes – https://orcid.org/0000-0001-6737-7775
Neil Coville – https://orcid.org/0000-0001-5370-1386

REFERENCES

1. Jelinek R. Carbon Quantum Dots. 1st ed. Cham, Switzerland: Springer International Publishing; 2017. p. 1–130. https://doi.org10.1007/978-3-319-43911-2.
2. Sciortino A, Cannizzo A, Messina F. Carbon Nanodots: A Review—From the current understanding of the fundamental photophysics to the full control of the optical response. J. Carbon Res. 2018;4(4):67–102. https://doi.org10.3390/c4040067.
3. Yuan F, Yuan T, Sui L, Wang Z, Xi Z, Li Y, Li X, Fan L, Chen A, Jin M et al. Engineering triangular carbon quantum dots with unprecedented narrow bandwidth emission for multicolored LEDs. Nat Commun. 2018;9(1):2249. https://doi.org10.1038/s41467-018-04635-5.
4. Roshni V, Gujar V, Pathan H, Islam S, Tawre M, Pardesi K, Santra MK, Ottoor D. Bioimaging applications of carbon dots (C. dots) and its cystamine functionalisation for the sensitive detection of Cr(VI) in aqueous samples. J Fluoresc. 2019;29:1381–1392. https://doi.org10.1007/s10895-019-02448-3.
5. Fan Z, Li S, Yuan F, Fan L. Fluorescent graphene quantum dots for biosensing and bioimaging. RSC Advances. 2015;5(25):19773–19789. https://doi.org10.1039/C4RA17131D.
6. Liu ML, Chen BB, Li CM, Huang CZ. Carbon dots: Synthesis, formation mechanism, fluorescence origin and sensing applications. Green Chem. 2019;21(3):449–471. https://doi.org10.1039/C8GC02736F.
7. Rani UA, Ng LY, Ng CY, Mahmoudi E. A review of carbon quantum dots and their applications in wastewater treatment. Adv Colloid Interface Sci. 2020;278:102124. https://doi.org10.1016/j.cis.2020.102124.
8. Han M, Zhu S, Lu S, Song Y, Feng T, Tao S, Liu J, Yang B. Recent progress on the photocatalysis of carbon dots: classification, mechanism and applications. Nano Today. 2018;19:201–218. https://doi.org10.1016/j.nantod.2018.02.008.
9. Chu KW, Lee SL, Chang CJ, Liu L. Recent progress of carbon dot precursors and photocatalysis applications. Polymers (Basel). 2019;11(4):689. https://doi.org10.3390/polym11040689.
10. Essner JB, Baker GA. The emerging roles of carbon dots in solar photovoltaics: A critical review. Environ Sci Nano. 2017;4(6):1216–1263. https://doi.org10.1039/C7EN00179G.
11. Fahmi MZ, Wibowo DLN, Sakti SCW, Lee HV, Isnaeni. Human serum albumin capsulated hydrophobic carbon nanodots as staining agent on HeLa tumor cell. Mater Chem Phys. 2020;239:122266. https://doi.org10.1016/j.matchemphys.2019.122266.
12. Gude V. Synthesis of hydrophobic photoluminescent carbon nanodots by using L-tyrosine and citric acid through a thermal oxidation route. Beilstein J Nanotechnol. 2014;5:1513–1522. https://doi.org10.3762/bjnano.5.164.
13. Lu L, Feng C, Xu J, Wang F, Yu H, Xu Z, Zhang W. Hydrophobic-carbon-dot-based dual-emission micelle for ratiometric fluorescence biosensing and imaging of Cu^{2+} in liver cells. Biosens Bioelectron. 2017;92:101–108. https://doi.org10.1016/j.bios.2017.01.066.
14. Bodik M, Siffalovic P, Nadazdy P, Benkovicova M, Markovic Z, Chlpik J, Cirak J, Kotlar M, Micusik M, Jergel M, et al. On the formation of hydrophobic carbon quantum dots Langmuir films and their transfer onto solid substrates. Diamond Related Materials. 2018;83:170–176. https://doi.org10.1016/j.diamond.2018.02.011.
15. Talib A, Pandey S, Thakur M, Wu HF. Synthesis of highly fluorescent hydrophobic carbon dots by hot injection method using Paraplast as precursor. Mater Sci Eng C. 2015;48:700–703. https://doi.org10.1016/j.msec.2014.11.058.
16. Shang W, Ye M, Cai T, Zhao L, Zhang Y, Liu D, Liu S. Tuning of the hydrophilicity and hydrophobicity of nitrogen doped carbon dots: A facile approach towards high efficient lubricant nanoadditives. J Mol Liq. 2018;266:65–74. https://doi.org10.1016/j.molliq.2018.06.042.
17. Yan L, Yang Y, Ma C-Q, Liu X, Wang H, Xu B. Synthesis of carbon quantum dots by chemical vapor deposition approach for use in polymer solar cell as the electrode buffer layer. Carbon. 2016;109:598–607. https://doi.org10.1016/j.carbon.2016.08.058.
18. Cui B, Yan L, Gu H, Yang Y, Liu X, Ma C-Q, Chen Y, Jia H. Fluorescent carbon quantum dots synthesised by chemical vapor deposition: an alternative candidate for electron acceptor in polymer solar cells. Opt Mater. 2018;75:166–173. https://doi.org10.1016/j.optmat.2017.10.010.
19. Yu H, Li X, Zeng X, Lu Y. Preparation of carbon dots by non-focusing pulsed laser irradiation in toluene. Chem Commun (Camb). 2016;52(4):819–822. https://doi.org10.1039/C5CC08384B.
20. Zhu Z, Wang S, Chang Y, Yu D, Jiang Y. Direct photodissociation of toluene molecules to photoluminescent carbon dots under pulsed laser irradiation. Carbon. 2016;105:416–423. https://doi.org10.1016/j.carbon.2016.04.047.
21. Vijaya Kumar Saroja AP, Garapati MS, Shyiamala Devi R, Kamaraj M and Ramaprabhu M. Facile synthesis of heteroatom doped and undoped graphene quantum dots as active materials for reversible lithium and sodium ions storage. Appl. Surf. Sci., 2020;504;144430. https://doi.org/10.1016/j.apsusc.2019.144430.
22. Coville NJ, Mhlanga SD, Nxumalo EN, Shaikjee A. A review of shaped carbon nanomaterials. S Afr J Sci. 2011;107(3/4):1–15. https://doi.org10.4102/sajs.v107i3/4.418.
23. Mutuma BK. Synthesis and characterisation of solid, hollow, core-shell and worm-like carbon nanostructures for applications in organic photovoltaic devices and chemical sensors, [PhD thesis]. Johannesburg: University of the Witwatersrand, South Africa. 2016.
24. Mutuma BK, Matsoso BJ, Ranganathan K, Keartland JM, Wamwangi D, Coville NJ. Generation of radical species in CVD grown pristine and N-doped solid carbon spheres using H_2 and Ar as carrier gases. RSC Advances. 2017;7(34):21187–21195. https://doi.org10.1039/C7RA03142D.
25. Xiong H, Motchelaho MA, Moyo M, Jewell LL, Coville NJ. Fischer-Tropsch synthesis: iron-based catalysts supported on nitrogen-doped carbon nanotubes synthesised by post-doping. Appl Catal A Gen. 2014;482:377–386. https://doi.org10.1016/j.apcata.2014.06.019.
26. Matsoso BJ, Ranganathan K, Mutuma BK, Lerotholi T, Jones G, Coville NJ. Time-dependent evolution of the nitrogen configurations in N-doped graphene films. RSC Advances. 2016;6(108):106914–106920. https://doi.org10.1039/C6RA24094A.
27. Atchudan R, Jebakumar Immanuel Edison TN, Perumal S, Vinodh R, Lee YR. Multicolor-emitting carbon dots from Malus floribunda and their

interaction with Caenorhabditis elegans. Mater Lett. 2020;261:127153. https://doi.org10.1016/j.matlet.2019.127153.

28. Faisal AD, Aljubouri AA. Synthesis and production of carbon nanospheres using noncatalytic CVD method. Int. J. Adv. Mater. Res. 2016;2:86–91.
29. Ferrari AC. Raman spectroscopy of graphene and graphite: Disorder, electron-, phonon coupling, doping and nonadiabatic effects. Solid State Commun. 2007;143(1-2):47–57. https://doi.org10.1016/j.ssc.2007.03.052.
30. Russo C, Apicella B, Ciajolo A. Blue and green luminescent carbon nanodots from controllable fuel-rich flame reactors. Sci Rep. 2019;9(1):14566. https://doi.org10.1038/s41598-019-50919-1.
31. Wen ZH, Yin XB. Excitation-independent carbon dots, from photoluminescence mechanism to single-color application. RSC Advances. 2016;6(33):27829–27835. https://doi.org10.1039/C5RA27172J.
32. Roy P, Chen P-C, Periasamy AP, Chen Y-N, Chang H-T. Photoluminescent carbon nanodots: synthesis, physicochemical properties and analytical applications. Mater Today. 2015;18(8):447–458. https://doi.org10.1016/j.mattod.2015.04.005.
33. Wang D, Wang Z, Zhan Q, Pu Y, Wang J-X, Foster NR, Dai L. Facile and scalable preparation of fluorescent carbon dots for multifunctional applications. Engineering (Beijing). 2017;3(3):402–408. https://doi.org10.1016/J.ENG.2017.03.014.
34. Bandi R, Gangapuram BR, Dadigala R, Eslavath R, Singh SS, Guttena V. Facile and green synthesis of fluorescent carbon dots from onion waste and their potential applications as sensor and multicolour imaging agents. RSC Advances. 2016;6(34):28633–28639. https://doi.org10.1039/C6RA01669C.
35. Pandey S, Mewada A, Thakur M, Tank A, Sharon M. Cysteamine hydrochloride protected carbon dots as a vehicle for the efficient release of the anti-schizophrenic drug haloperidol. RSC Advances. 2013;3(48):26290–26296. https://doi.org10.1039/c3ra42139b.
36. Mokoloko LL, Matsoso BJ, Forbes RP, Barrett DH, Moreno BD, Coville NJ. Evolution of large-area reduced graphene oxide nanosheets from carbon dots via thermal treatment. Carbon Trends. 2021;4:100074. https://doi.org10.1016/j.cartre.2021.100074.
37. Mewada A, Pandey S, Shinde S, Mishra N, Oza G, Thakur M, Sharon M, Sharon M. Green synthesis of biocompatible carbon dots using aqueous extract of Trapa bispinosa peel. Mater Sci Eng C. 2013;33(5):2914–2917. https://doi.org10.1016/j.msec.2013.03.018.
38. Mongwe TH, Matsoso BJ, Mutuma BK, Coville NJ, Maubane MS. Synthesis of chain-like carbon nano-onions by a flame assisted pyrolysis technique using different collecting plates. Diamond Related Materials. 2018;90:135–143. https://doi.org10.1016/j.diamond.2018.10.002.
39. Sarkar S, Banerjee D, Ghorai UK, Das NS, Chattopadhyay KK. Size dependent photoluminescence property of hydrothermally synthesised crystalline carbon quantum dots. J Lumin. 2016;178:314–323. https://doi.org10.1016/j.jlumin.2016.05.033.
40. Xia C, Zhu S, Feng T, Yang M, Yang B. Evolution and synthesis of carbon dots: from carbon dots to carbonized polymer dots. Adv Sci (Weinh). 2019;6(23):1901316. https://doi.org10.1002/advs.201901316.
41. Tian M, Liu BS, Hammonds M, Wang N, Sarre PJ, Cheung AS-C. Formation of polycyclic aromatic hydrocarbons from acetylene over nanosized olivine-type silicates. Phys Chem Chem Phys. 2012;14(18):6603–6610. https://doi.org10.1039/c2cp23309f.
42. Bensabath T, Le MD, Monnier H, Glaude PA. Polycyclic aromatic hydrocarbon (PAH) formation during acetylene pyrolysis in tubular reactor under low pressure carburising conditions. Chem Eng Sci. 2019;202:84–94. https://doi.org10.1016/j.ces.2019.03.030.
43. Ono K, Yanaka M, Saito Y, Aoki H, Fukuda O, Aoki T, Yamaguchi T. Effect of benzene-acetylene compositions on carbon black configurations produced by benzene pyrolysis. Chem Eng J. 2013;215–216:128–135. https://doi.org10.1016/j.cej.2012.10.085.
44. Panickar R, Sobhan CB, Chakravorti S. Chemical vapor deposition synthesis of carbon spheres: effects of temperature and hydrogen. Vacuum. 2020;172:109108. https://doi.org10.1016/j.vacuum.2019.109108.
45. Deshmukh AA, Mhlanga SD, Coville NJ. Carbon spheres. Mater Sci Eng Rep. 2010;70(1-2):1–28. https://doi.org10.1016/j.mser.2010.06.017.

SUPPLEMENTARY MATERIAL TO:

The simultaneous synthesis of carbon dots and carbon spheres with tuneable sizes using a vertical chemical vapour deposition method

LL Mokoloko, RP Forbes and NJ Coville

S Afr J Chem, 2022, 76, 25–30
https://doi.org/10.17159/0379-4350/2022/v76a05

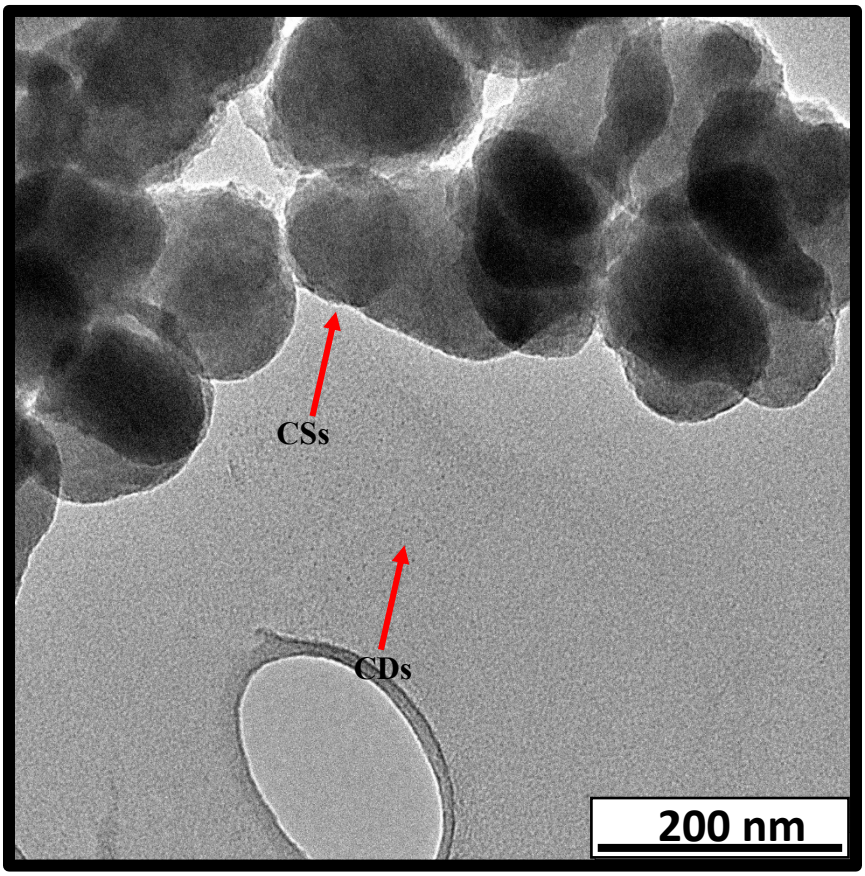

Figure S1: TEM image of products obtained in SCC#2 before purification

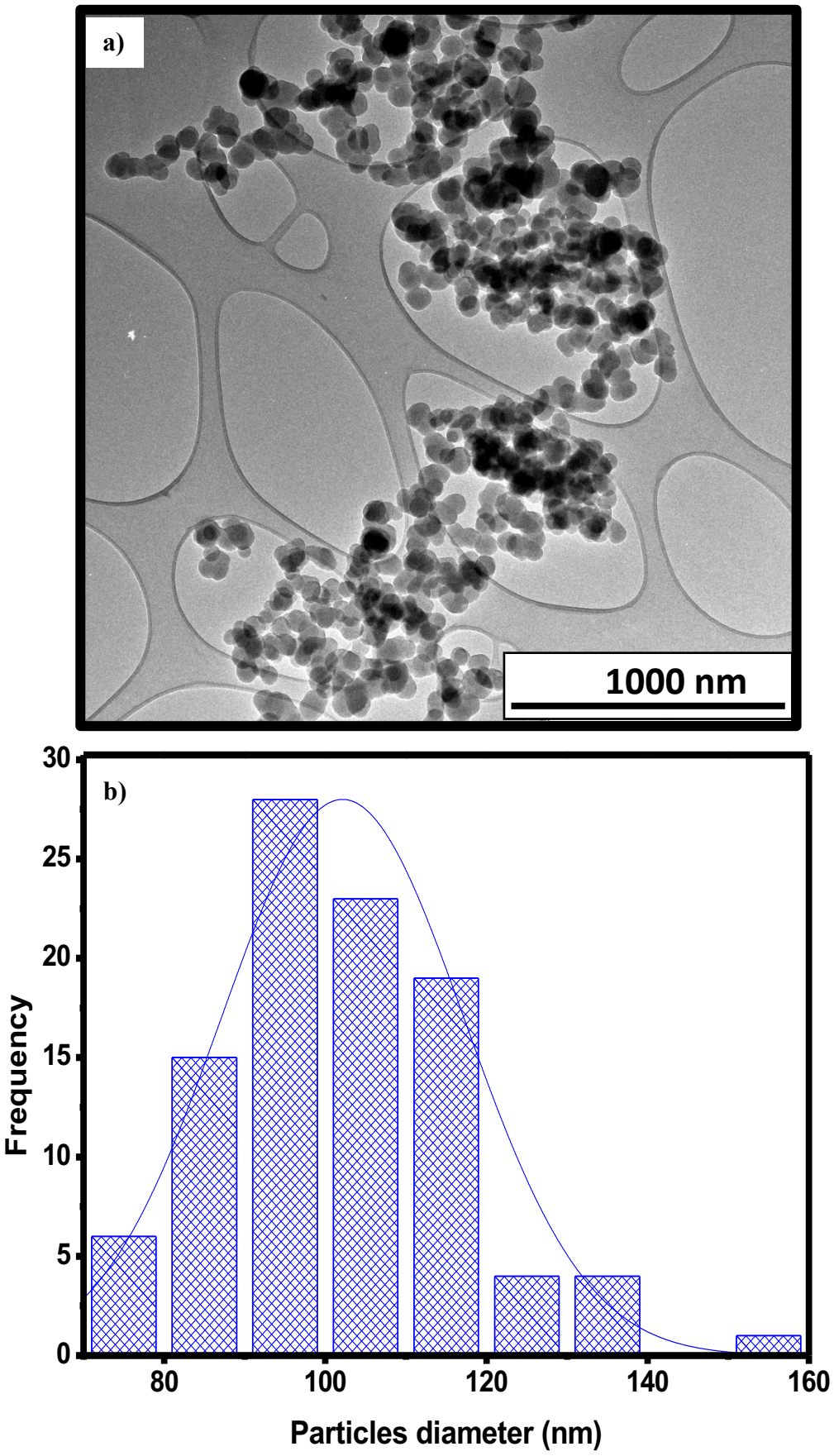

Figure S2: a) TEM image and **b)** particle size distribution histogram and a normal distribution curve of the $CSs_{600/10/1}$ sample

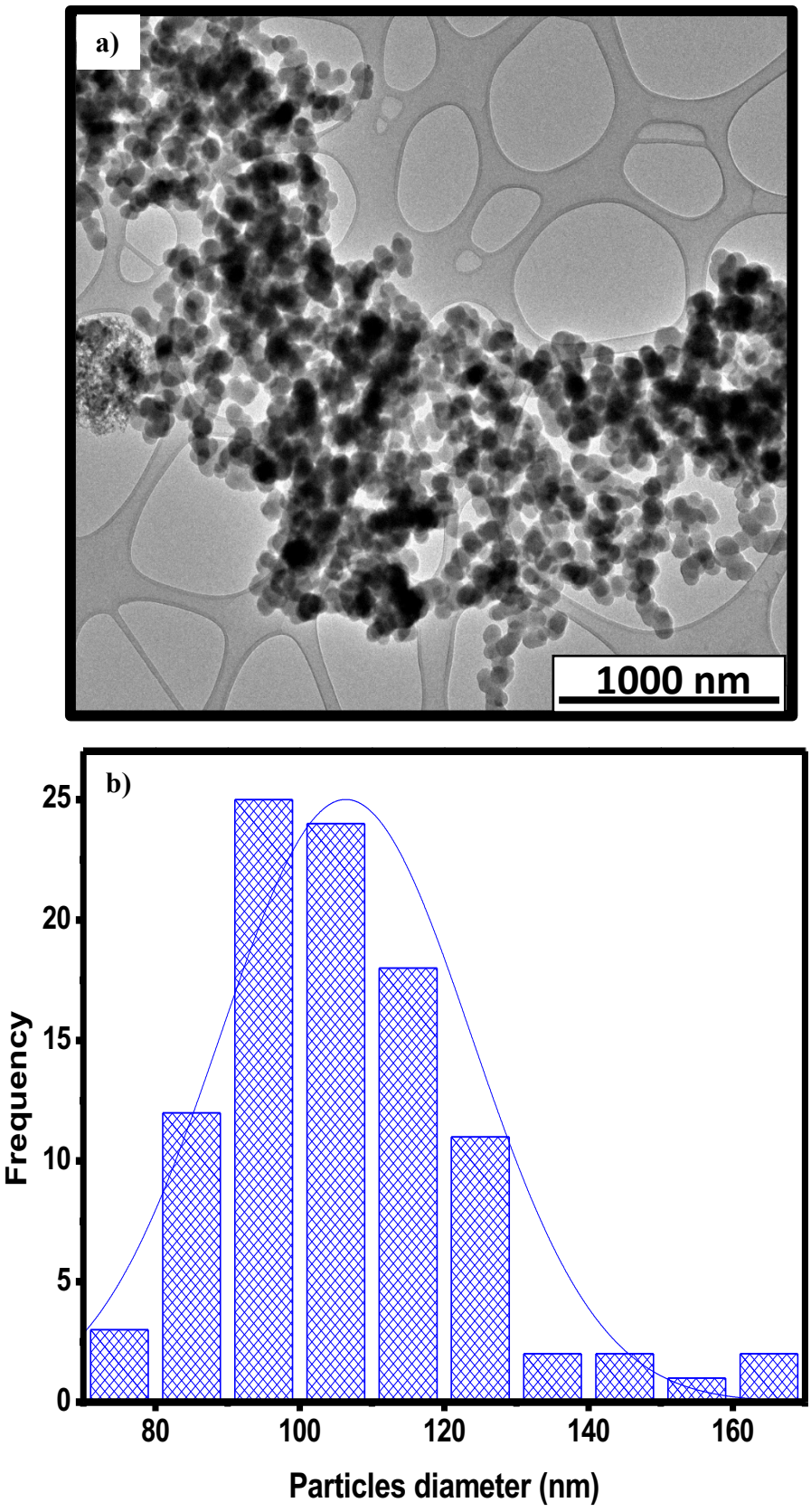

Figure S3: a) TEM image and **b)** particle size distribution histogram and a normal distribution curve of the $CSs_{550/10/1}$ sample

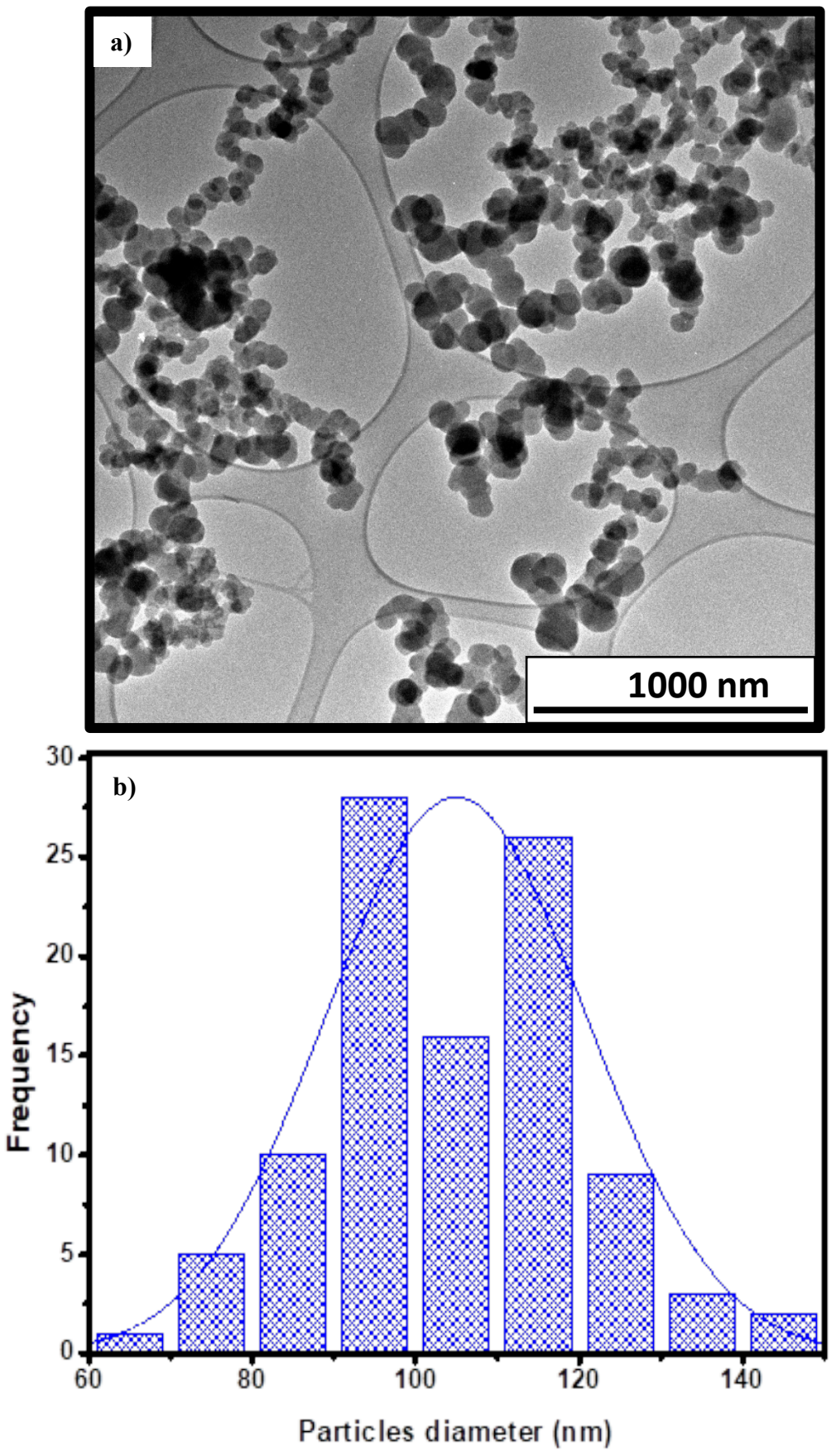

Figure S4: a) TEM image and **b)** particle size distribution histogram and a normal distribution curve of the $CSs_{520/10/1}$ sample

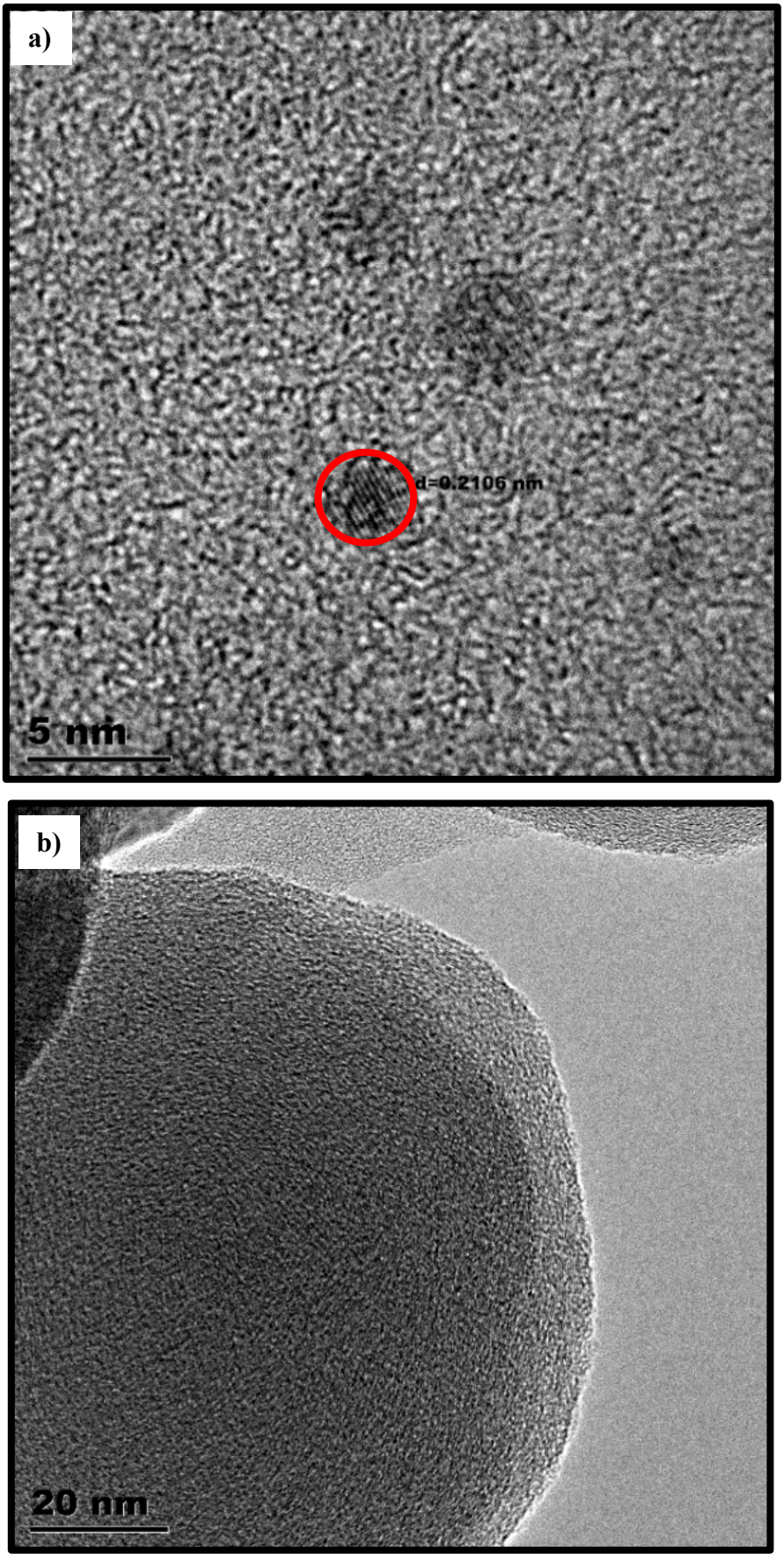

Figure S5: HRTEM images of **a)** $CDs_{600/10/2}$ showing their lattice fringes **b)** $CSs_{600/10/1}$ sample

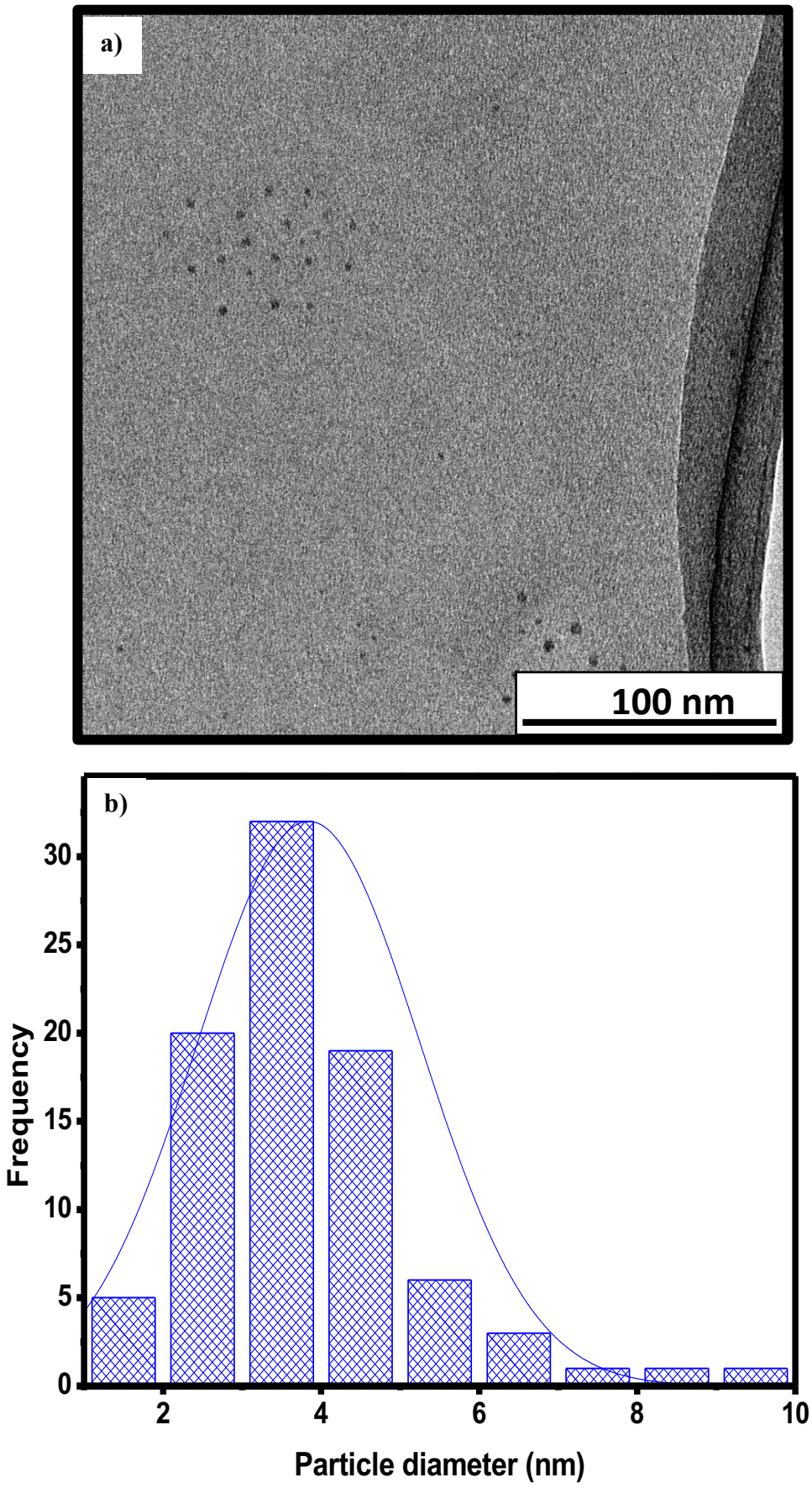

Figure S6: a) TEM image and **b)** particle size distribution histogram and a normal distribution curve of the $CDs_{600/9/2}$ sample

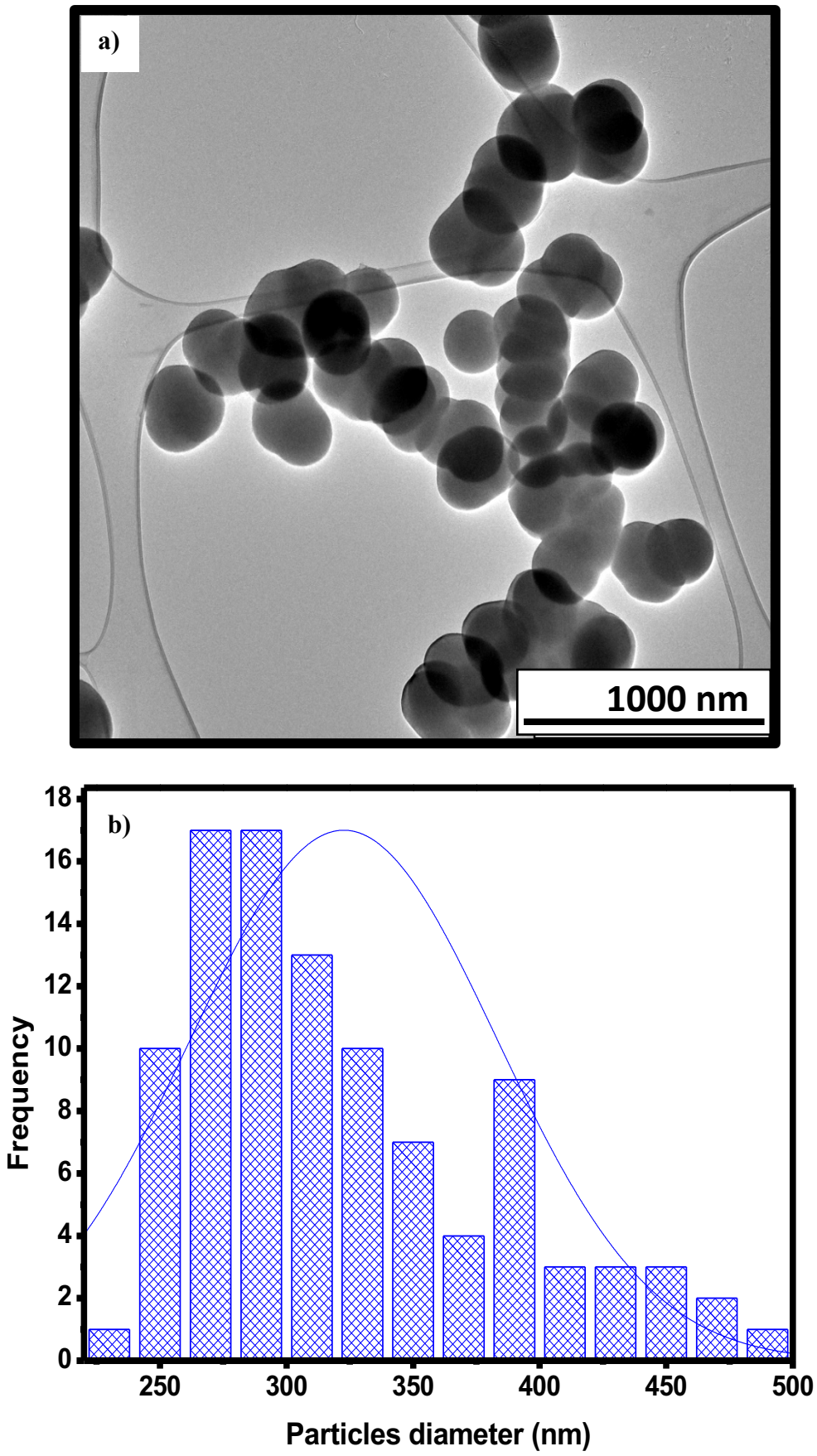

Figure S7: a) TEM image and **b)** particle size distribution histogram and a normal distribution curve of the $CSs_{400/8/1}$ sample

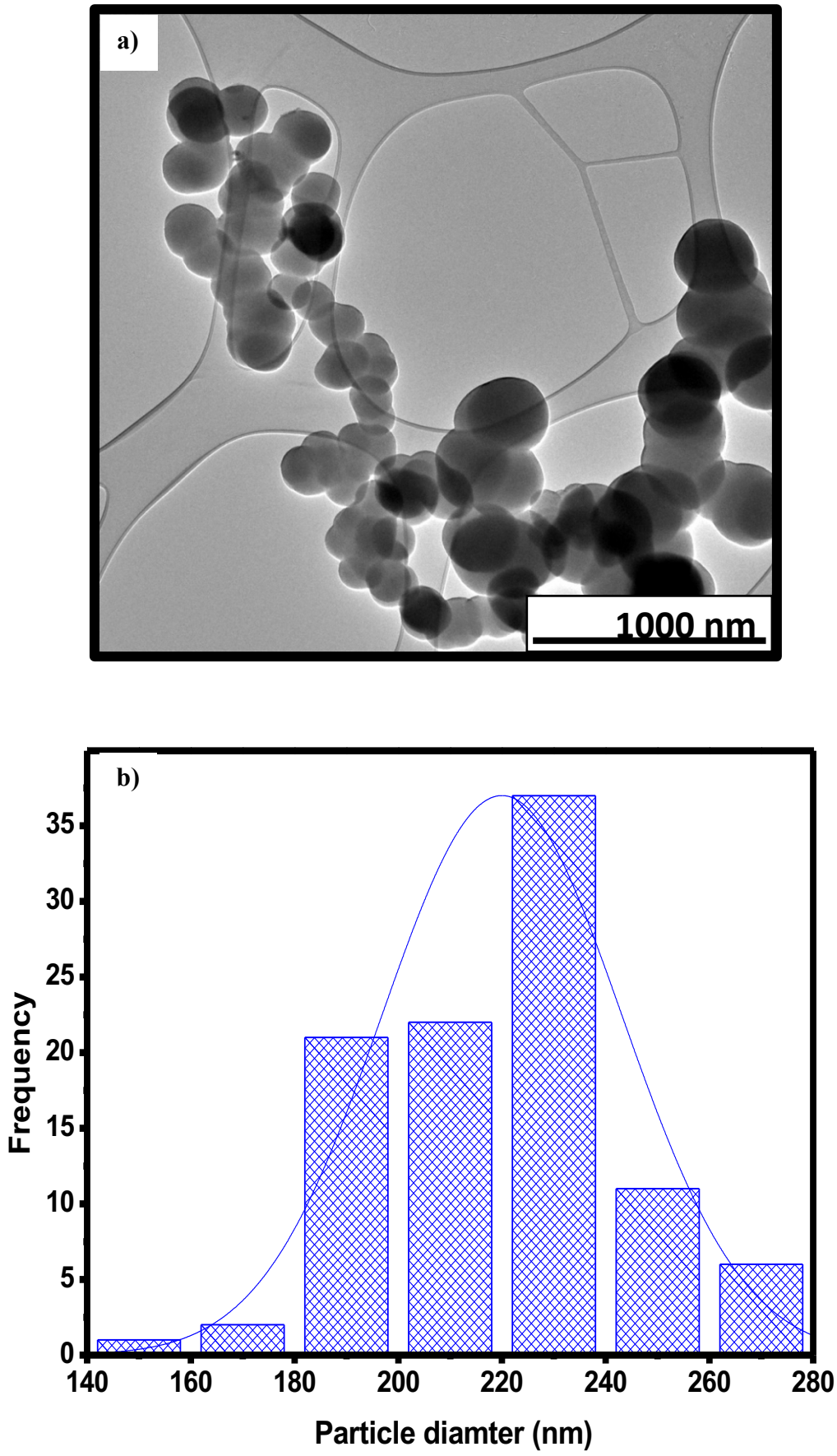

Figure S8: a) TEM image and **b)** particle size distribution histogram and a normal distribution curve of the $CSs_{400/8/2}$ sample

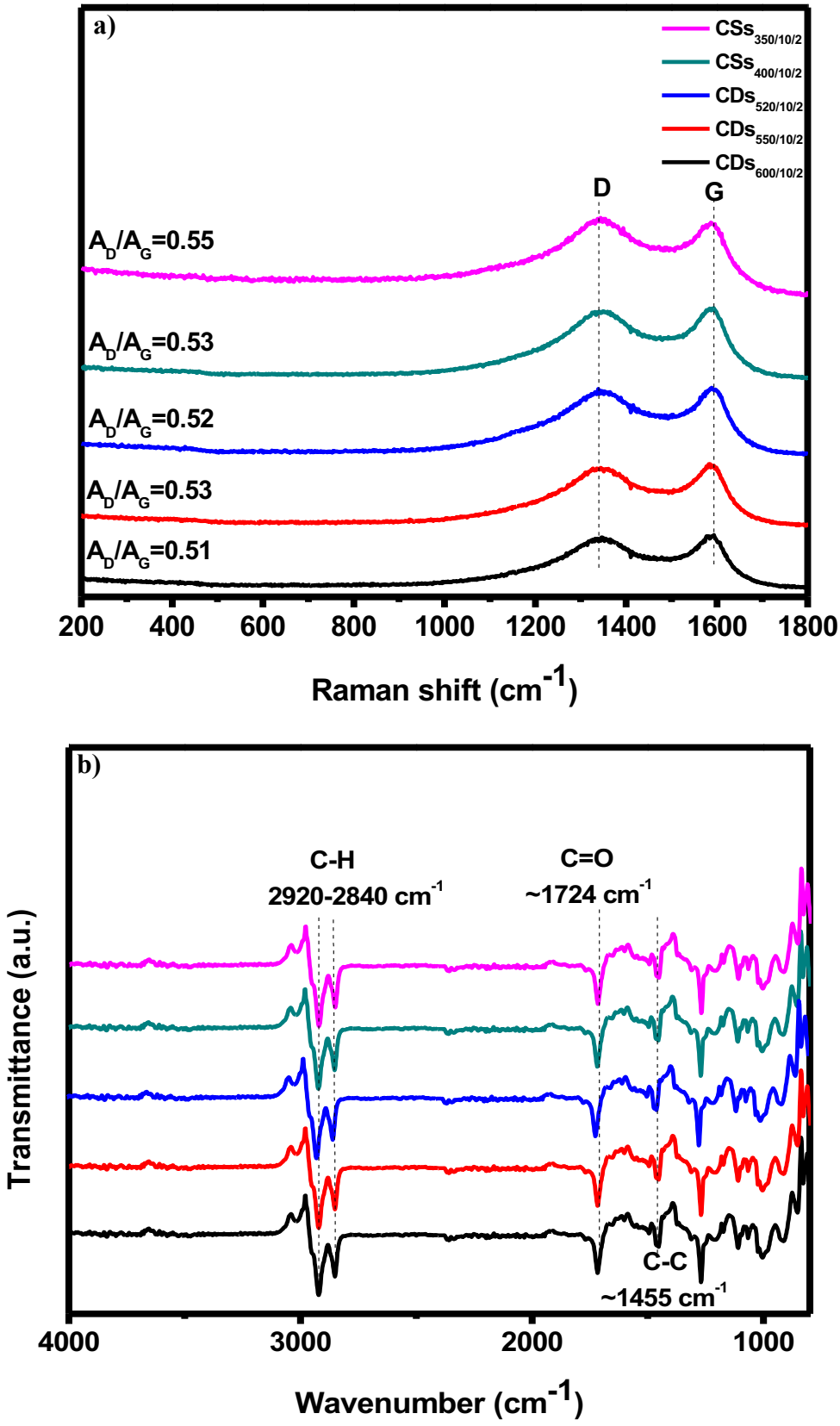

Figure S9: **a)** Raman spectra and **b)** FTIR spectra of $CDs_{520/10/2}$, $CDs_{550/10/2}$ and $CDs_{600/10/2}$, $CSs_{400/10/2}$ and $CSs_{350/10/2}$ samples

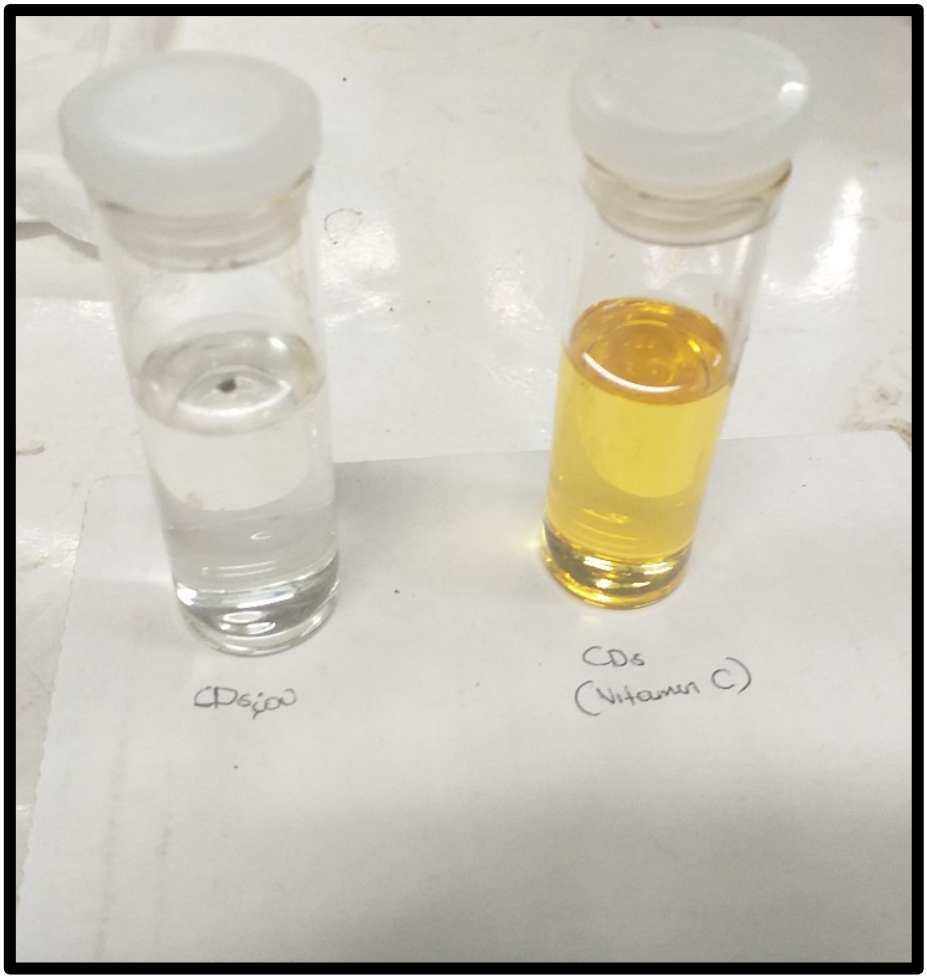

Figure S10: **a)** sample CDs_{600} synthesised in the current study and **b)** CDs synthesised from vitamin C in distilled water

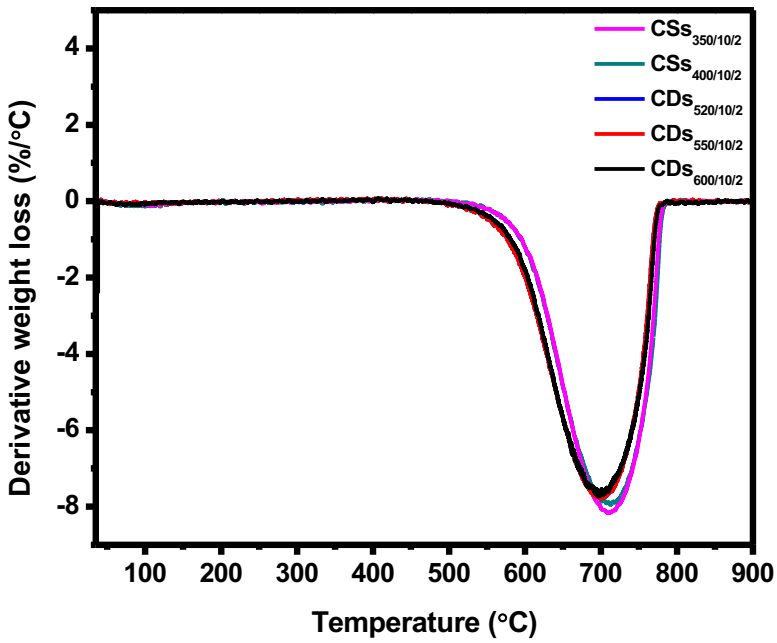

Figure S11: Derivative weight loss thermograms of the samples synthesized at 1000 °C